Kahramanmaras, Turkey Earthquake on 6th February 2023- A case study on Sentinel data using Snap Software

Vijay A.[1]*, Saravanavel J.[1], Vasudevan S.[2], Ramasamy S.M.[1] and Kumanan C.J.[1]
1. Dept. of Remote Sensing, Bharathidasan University, Tiruchirappalli-623023, Tamil Nadu, INDIA
2. Dept. of Earth Sciences, Annamalai University, Chidambaram- 608002, Tamil Nadu, INDIA
*vijayvasanthgeo@gmail.com

Abstract

In the recent era, our earth has become more prone for various disasters like Earthquake, Tsunami, Cyclones etc. Earthquakes are the most devastating natural disasters, causing significant loss of life, damage to infrastructure and long-term economic and social consequences. This study delves earthquake that struck Kahramanmaras, Turkey, on February 6, 2023, registering a magnitude of 7.8 and significantly impacted southeastern Turkey and northern Syria. The earthquake-affected zone, based on model estimates, spanned roughly 350,000 square kilometers, experiencing extensive destruction. Estimates indicate that up to 9.1 million people were directly impacted, with several million rendered homeless. In Turkey, nearly 46,000 people lost their lives, with the provinces of Hatay and Kahramanmaras being the hardest hit, reporting about 21,900 and 12,600 deaths respectively.

Turkey's Disaster and Emergency Management Presidency (AFAD) noted that approximately 280,000 buildings were either severely damaged or collapsed, while an additional 710,000 structures suffered major damage.

In this continuation the focal point of this study is the application of remote sensing technologies, such as synthetic aperture radar (SAR) and optical satellite imagery to assess earthquake-induced changes in land surface deformation and infrastructure damage. The use of satellite data allows for rapid damage assessment, facilitating efficient disaster response and recovery efforts. This case study underscores the importance of integrating satellite-based remote sensing with ground-based data to provide a comprehensive assessment of earthquake impacts.

The findings not only contribute to the understanding of seismic hazards in the region but also demonstrate the potential of Sentinel data, processed through SNAP, in improving disaster response strategies, hazard mapping and infrastructure planning in earthquake-prone areas like Kahramanmaras.

Keywords: Kahramanmaras, Earthquake, Sentinel-1, SNAP.

Introduction

In the modern era world, earthquakes and seismic activities are increasing more and can cause significant damage in various ways including loss of life and property. The destruction of infrastructure, homes and communities is serious consequence of these natural events. Advances in seismic technology and engineering are helping to mitigate some of these impacts by enhancing building designs and developing early warning systems. Despite these efforts, ongoing research and preparedness are crucial for reducing their overall impact. Turkey is particularly vulnerable to earthquakes because it is situated in a top several significant seismic fault lines[4], including the North Anatolian Fault[10], which is one of the most active and dangerous fault lines in the world[5].

Over the last two decades, this geological positioning has resulted in Turkey and its surrounding territories experiencing numerous earthquakes at regular intervals[8,15]. These earthquakes typically range in magnitude from 6 to 7, causing substantial concern due to their potential for significant destruction and loss of life. The frequency and intensity of these seismic events underscore the ongoing risk that Turkey faces as a result of its geologically active location. On February 6, 2023, a devastating earthquake with a magnitude of 7.8 struck with its epicenter situated just south of the Turkish city of Kahramanmaras. The initial quake caused widespread destruction and shortly afterward, a severe aftershock occurred near the border that separates southern Turkey from northern Syria, further exacerbating the damage in both regions.

The magnitude 7.8 earthquake struck at 4:17 a.m. local time, with its epicenter located approximately 24 km (15 miles) south of Kahramanmaras and a similar distance northwest of Gaziantep, in south-central Turkey. The quake's focus was at a shallow depth of just 10 km (6.2 miles) below the surface[9,16]. About 11 minutes later, a magnitude of 6.7 aftershock occurred near the same location. Nine hours later, at 1:24 p.m., a second major seismic event, a magnitude-7.7 aftershock, struck 48.3 km (30 miles) northwest of Kahramanmaras and about 32 km (20 miles) south of Elbistan. Both of these major seismic events occurred within the East Anatolian Fault Zone, which traversed south-eastern Turkey and serves as the boundary between the Arabian and Eurasian tectonic plates.

The smaller Anatolian Plate is flanked by the East Anatolian fault zone to the south and the North Anatolian fault along Turkey's Black Sea coast. At the boundary between the

Anatolian and Arabian plates, the Arabian plate is moving northward at a rate of about 16 mm (1.9 inches) per year, generating horizontal compression that slowly drives the Anatolian plate westward[11,12]. The East Anatolian fault zone consists of strike-slip faults, where rock masses slide past one another[13]. At the location of the earthquake's focus, the fault plane was nearly vertical[14] and the compressive forces caused one side of the fault to slip approximately 8 meters (26.2 feet) along a 300-km front. The magnitude-7.7 aftershock struck along the Cardak and Dogansehir faults farther north, shifting the ground by up to 11 meters (36 feet) along a 180-km front.

Study Area

Kahramanmaras is a city in southern Turkey, nestled at the edge of a fertile plain below Ahır mountain, to the east-northeast of Adana. The city lies near the southern gateways of three major passes through the Taurus mountains, connecting it to Goksun, Elbistan and Malatya. The city center is situated 568 meters above sea level. The Ceyhan River, which originates from the mountains encircling the Elbistan plain, is the city's most significant hydrological feature. Kahramanmaras is a focal point for light industry and trade, specializing in the production and export of olive oil, spices and hand-woven textiles. The region around Kahramanmaras is mountainous and abundant in minerals, particularly iron and silver. Its fertile agricultural land, nourished by the Ceyhan River, produces wheat, rice and legumes.

Geology of the study area: The geology of southern Turkey is intricate and varied, influenced by its location at the junction of several tectonic plates: the Eurasian, African and Arabian plates. This region, especially the Eastern Mediterranean area, is geologically dynamic, with a rich array of rock formations, fault systems and geological structures[2].

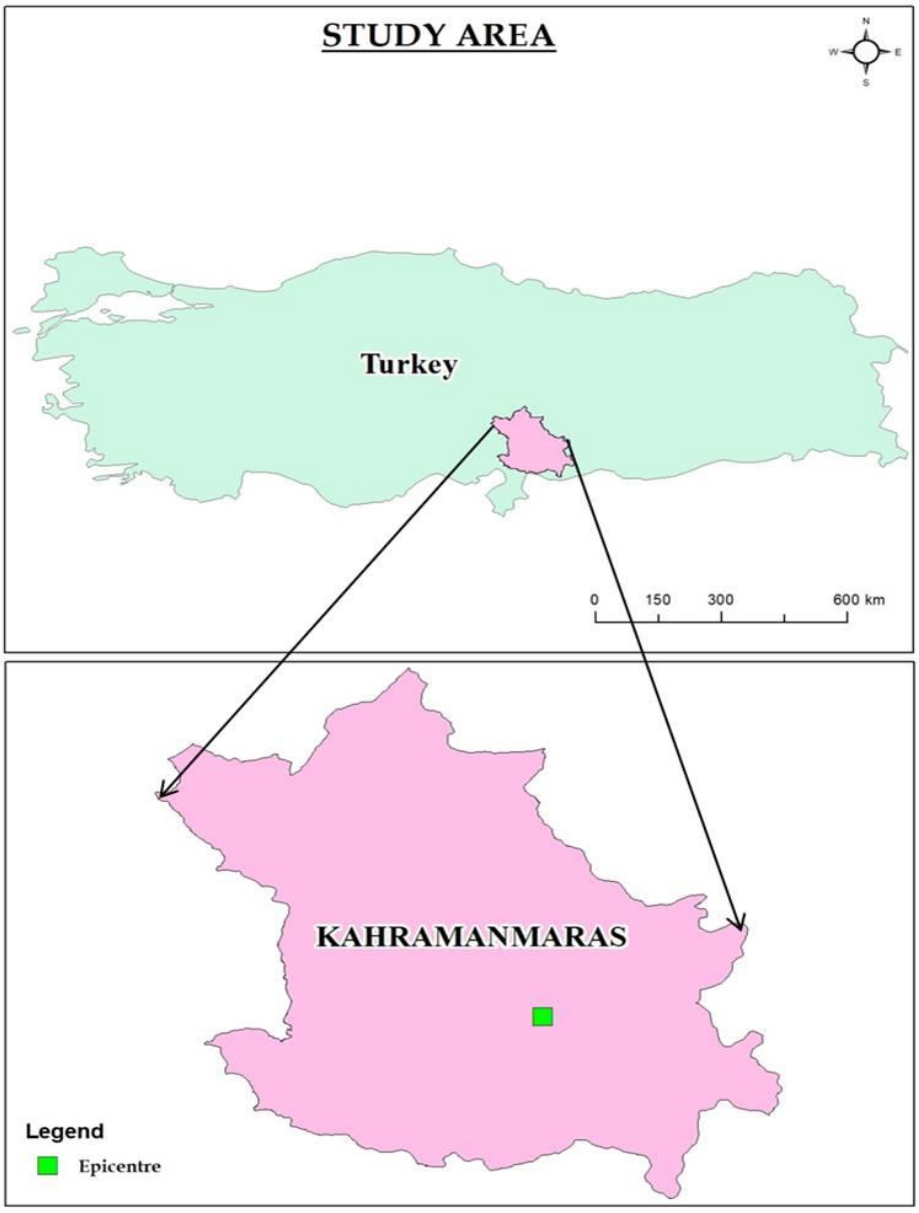

Fig. 1: Study Area

Southern Turkey is predominantly underlain by sedimentary rock formations that span a vast geological timeline, extending from the Mesozoic era, approximately 250 to 66 million years ago, to the Cenozoic era, which began around 66 million years ago and continues to the present day. These sedimentary layers are composed mainly of limestone, sandstone and shale. These rocks were originally deposited in ancient marine environments, reflecting periods when the region was submerged under shallow seas. The region is characterized by numerous folds and thrust faults resulting from the compressional tectonic forces. These structures have created complex mountain ranges and valleys. Southern Turkey is rich in various minerals, including chromite, copper and marble. The Eastern Mediterranean basin, which includes parts of southern Turkey, is believed to contain significant hydrocarbon reserves, particularly natural gas.

Tectonics of the study area: Southern Turkey is located on the Anatolian plate, a microplate positioned between the larger Eurasian, African and Arabian plates. The converging movements of these surrounding plates exert significant tectonic stress on the Anatolian plate, leading to a dynamic geological environment characterized by mountain formation, faulting and frequent seismic activity[6]. A key feature in this region is the East Anatolian Fault Zone (EAFZ), a major strike-slip fault that marks the boundary between the Anatolian and Arabian plates. This fault system is a primary source of the region's seismic events, with the lateral movements along the fault contributing to southern Turkey's complex geological landscape.

Additionally, to the south of Turkey, the Hellenic and Cyprus Arcs represent critical subduction zones where the African plate is being subducted beneath the Eurasian plate. This process has created a variety of intricate geological features, including deep-sea trenches and volcanic arcs and is responsible for much of the volcanic activity in the Eastern Mediterranean.

Material and Methods

Software and Materials: Nowadays land deformations like landslides, earthquakes etc. are mapped by using various platforms. SNAP (Sentinel Application Software) is a software tool used to map the Sentinel data[1,3,7,17]. These Sentinel data are downloaded from European Space Agency (esa-science hub) (https://scihub.copernicus.eu/). In this study, we discussed about the Turkey earthquake caused in 2023 using the Sentinel-1 data for this calibration. The Sentinel-1 data was downloaded for past and postdates of the events (28.01.2023 and 09.02.2023) by which we calibrated the deformations on the area. SLC product type are taken for the analysis with acquisition mode of 'IW'. Ascending data with 'VV' type polarization data are used.

The data downloaded are:
S1A_IW_SLC__1SDV_20230128T153424_20230128T153451_046986_05A2B6_00C8- Past Event
S1A_IW_SLC__1SDV_20230209T153423_20230209T153450_047161_05A88A_9FEC-Post Event

Methodology: In the SNAP desktop we may build three graphs for the analysis of the detection of deformation on the Turkey area, the graph was built by clicking the tools-graph builder on the task bar of the SNAP desktop. At first build the graph for preprocessing process is like apply orbit file option etc.

Graph I: This is the preprocessing technique of Sentinel data for the preparation of the analysis. In this process, the past and post data are separately gone for the topsar split and applying orbit file (Table 1). The S-1 Tops Split is utilized to isolate the specific bursts needed for the analysis. Currently, each Sub-Swath is processed separately. If the area of interest extends across multiple Sub-Swaths, they should be merged afterward using the S-1 Tops Merge operator shown in fig. 2A. In this analysis, we take IW3, VV processing parameters for the analysis.

Orbit auxiliary data hold crucial information about the satellite's position at the time SAR data is acquired. In the case of Sentinel-1 products, these orbit files are automatically retrieved by SNAP and integrated into the product's metadata. This integration is accomplished using the Apply Orbit File operator, which can be accessed through the Radar menu. This step ensures that the satellite's precise position is accurately reflected in the data, which is essential for subsequent processing and analysis. The output of the first graph was shown in fig. 2B.

Graph II: After the completion of the preprocessing of the two images, they had undergone for Graph-II starts with Back Geocoding in SNAP is a critical process (Table 2) for the coregistration of radar images, particularly those from Sentinel-1 SAR. This process involves aligning two or more radar images to a common geometry, typically using a master image (past event image) as a reference. The coregistration achieved through back geocoding ensures that corresponding pixels in the images represent the same ground location, which is essential for tasks like interferometric analysis, change detection and multi-temporal analysis. The process relies on precise orbit information, which describes the satellite's position and velocity during image acquisition and this information is used to accurately calculate the location of each pixel in the radar images. Additionally, a Digital Elevation Model (DEM) is incorporated to correct for distortions caused by the Earth's topography, ensuring the images are correctly aligned with surface features.

SNAP employs the Range-Doppler method, a widely used technique for SAR data, to align the images based on range and Doppler frequency. This step is crucial for applications requiring precise pixel matching, such as interferometric SAR (InSAR) for detecting ground displacement. SNAP simplifies this process by automatically downloading the

necessary DEM from online sources, ensuring the use of the most suitable elevation data; in this process we selected SRTM DEM (Fig.3) for the process.

The Enhanced Spectral Diversity (ESD) operator is an important step that follows the Back Geocoding process in the processing of radar data. After the initial alignment of images through Back Geocoding, the ESD operator refines this alignment by focusing on the overlapping regions between adjacent bursts within the radar data. These overlapping areas contain valuable spectral information that ESD exploits to further enhance the accuracy of the coregistration. Specifically, ESD analyzes the spectral diversity in these regions to detect and correct any residual misalignments. It performs precise range and azimuth corrections for each burst individually, ensuring that all parts of the image are accurately aligned. This process is crucial for improving the overall quality of the coregistered images, leading to better results in subsequent analyses, such as interferogram or change detection. After the ESD process, the images undergo for interferograms process. At this stage, we will generate an interferogram using the interferometric pair, consisting of the master and slave images, while also estimating the coherence from the stack of coregistered complex images. This step is crucial for analyzing the phase differences between the two images, which can reveal subtle ground movements. Once the interferogram and coherence estimation are completed, the next step is to connect the Interferogram operator to the Enhanced Spectral Diversity (ESD) operator. This connection allows for further refinement of the alignment and ensures that the generated interferogram is as accurate as possible.

We then proceed with the Sentinel-1 TOPSAR Deburst. During this stage, each subswath image, which consists of a series of bursts processed as individual Single Look Complex (SLC) images, is integrated. The individually focused burst images are arranged in azimuth-time order and combined into a single sub-swath image, with black-fill used to determine the boundaries between bursts.

Table 1
Graph-1

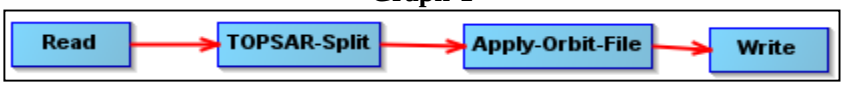

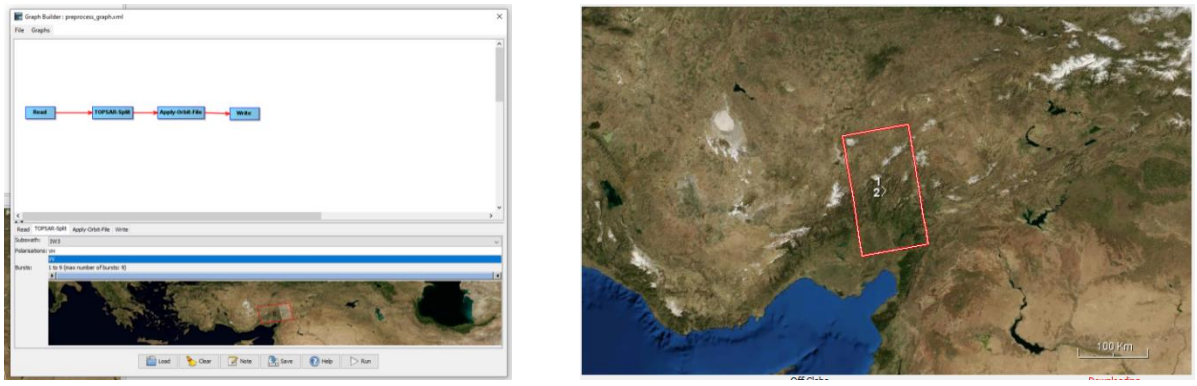

(A) **(B)**

Fig. 2: (A) S-1 Tops split processes showing the sub-swath classifications; (B) Output of the Process.

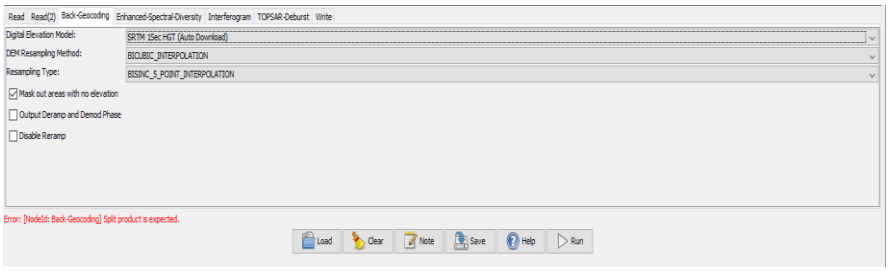

Fig. 3: Processing window of Graph-II- Back-geocoding on SNAP desktop.

Table 2
Graph-II

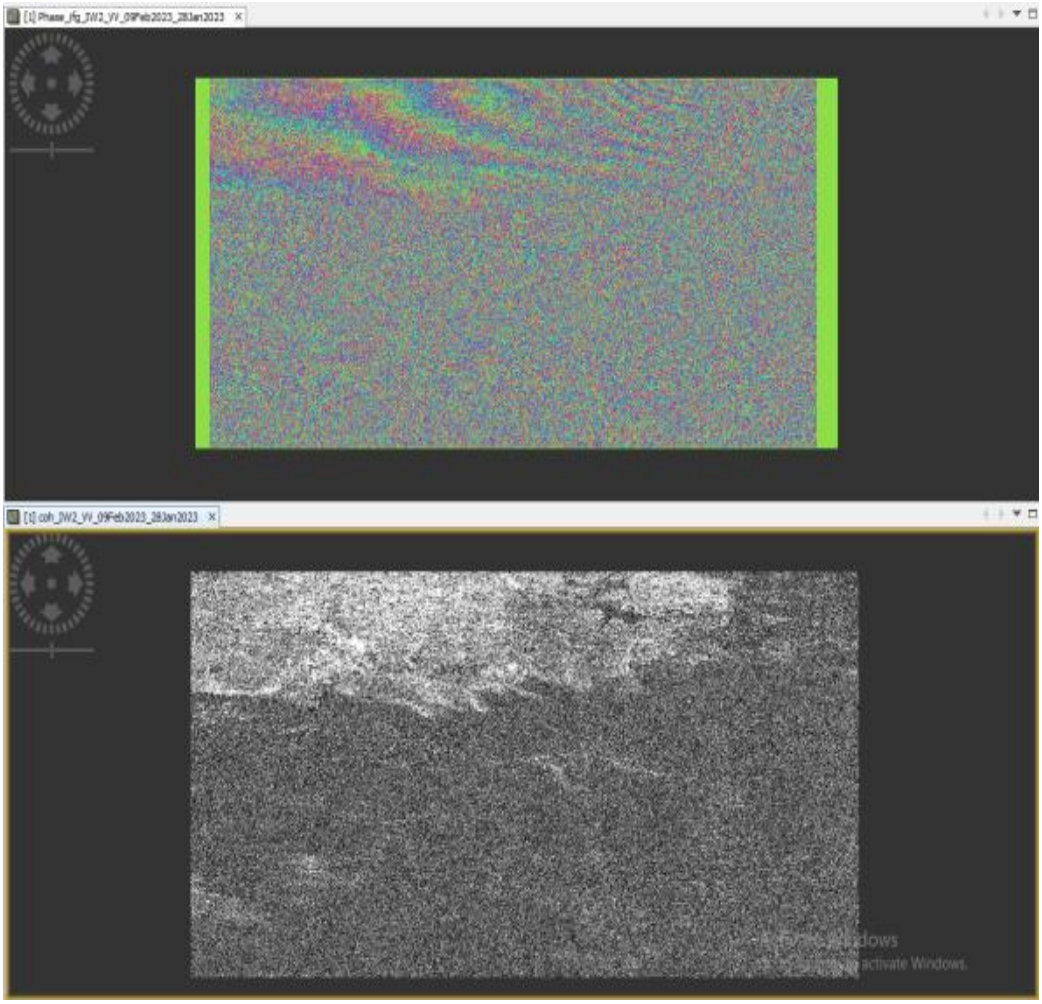

Fig. 4: Output Phase and Coherence images of Graph-II process.

This method ensures continuous ground coverage due to the sufficient overlap between adjacent bursts and sub-swaths. Finally, all burst images from every sub-swath are resampled to a consistent pixel spacing grid in both range and azimuth directions, while maintaining the phase information. Fig. 4 shows the outcome of the process as phase and coherence.

Graph III: The third and last graph involves major portion of analysis in the process which consists of topographic phase removal, multilooking, filtering and export process done in this graph. Removing the phase variations is caused by topography from the debursted interferogram. This phase, known as topographically induced phase, results from the elevation differences in the terrain and can distort the true radar signal. By correcting for these topographic effects, we ensure that the interferogram accurately reflects only the phase differences related to surface changes, rather than the underlying topographic features. This correction is crucial for obtaining reliable results in subsequent analyses, such as detecting ground displacement or changes.

After the topophase removal, we enter into the multilook table, the original SAR image is prone to inherent speckle noise, random variations in pixel intensity that can obscure meaningful details, multilook processing is implemented at this stage to mitigate this issue. Multilook processing involves averaging multiple looks or views of the same scene to reduce the speckle noise. This technique smooths out the noise while preserving the underlying image features, thereby enhancing the overall clarity and interpretability of the image. By doing this, the resultant image becomes more visually coherent and easier to analyze, allowing for more accurate interpretation and subsequent analysis.

After removing the speckle noise in multilook tab, we may forwarded into the filtering, in this process we did Goldstein Phase filtering for the above processed outputs. In SAR interferometry, phase noise can degrade the quality of the interferogram, which represents the phase difference between two SAR images. The Goldstein phase filter is a method used to reduce phase noise while preserving the phase information critical for producing high-quality interferograms. This filtering is particularly important in areas with low coherence, where noise dominates over the signal, like over water bodies, vegetation, or urban areas with rapid change.

In this filtering we assigned the FFT size, kernel size and threshold values as 64, 3 and 0.2 respectively as default. We may change those values accordingly our need. The final

step in this segment of the processing workflow is the export of data specifically for SNAPHU (Statistical-cost Network-flow Algorithm for Phase Unwrapping) processing. This export is necessary to perform phase unwrapping, a key procedure in interferometric and signal processing. Phase unwrapping is essential because it addresses the inherent ambiguities in wrapped phase data by reconstructing a continuous phase signal. Without this step, the raw data remains ambiguous, limiting its usability for further analysis.

Phase unwrapping involves converting the wrapped phase values, which are constrained within a range (e.g., $-\pi$ to $+\pi$), into a smooth, continuous phase surface, allowing for accurate interpretation of the interferometric measurements. This process is particularly important in remote sensing, radar and optical applications, where precise phase information is needed to analyze terrain, deformation, or other physical properties.

For those seeking an in-depth understanding of phase unwrapping theory and algorithms, the works by Ghiglia and Pritt provide a comprehensive exploration of the subject, offering both mathematical foundations and practical applications. Additionally, Constantini's contributions to the field further enhance the theoretical framework, providing additional context and advancements in phase unwrapping techniques. These references are invaluable for a thorough grasp of the complexities involved in phase unwrapping.

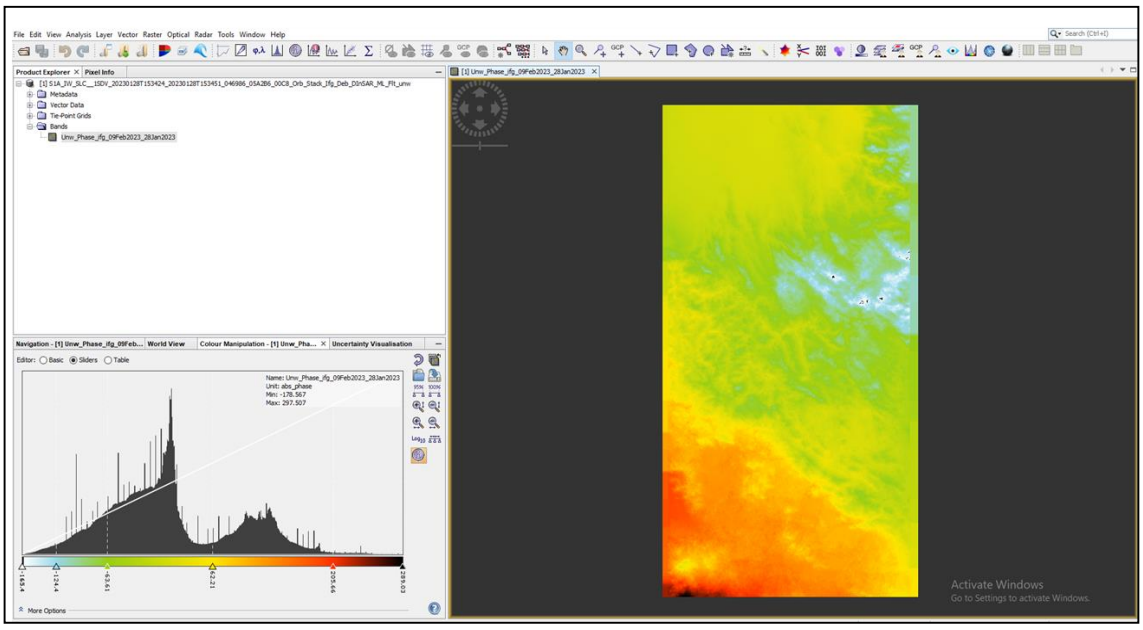

Fig. 5: Output of Graph-III.

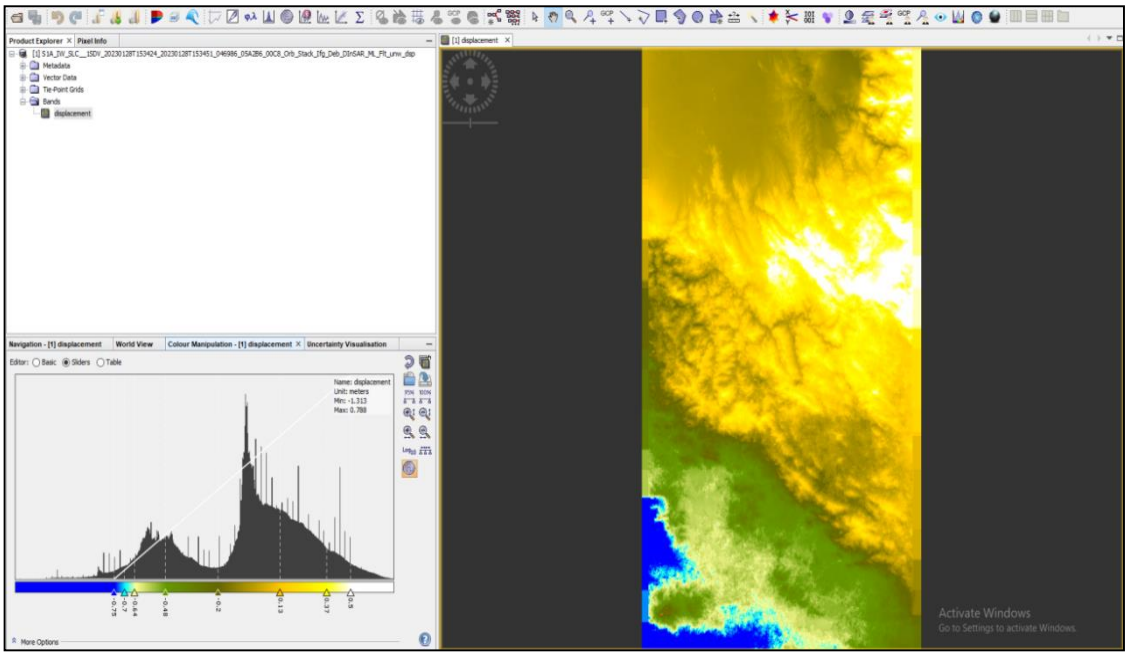

Fig. 6: Processed output of the interferometric phase to displacement phase.

Results and Discussion

After the completion of all the three graphs, we are at the point to proceed with phase unwrapping via SNAPHU. To begin, open a Linux terminal and navigate to the following directory:

"S1A_IW_SLC__1SDV_20230128T153424_20230128T153451_046986_05A2B6_00C8_Orb_Stack_Ifg_Deb_DInSAR_ML_Flt"

Once there, locate and open the configuration file named snaphu.conf. Inside this file, you will find the necessary command to initiate SNAPHU. Now, open configuration file "snaphu. conf" and copy "command to call snaphu": snaphu -f snaphu. conf Phase_ifg_VV_27Jul2015_15Feb2023. snaphu.img 2959 and paste it in the terminal. Also, in the "Output Files" use the comment (#) before "LOGFILE". Proceed by executing the command. The results are stored in the above-mentioned folder.

The SNAPHU import processing is employed to generate a refined interferometric product by resolving the ambiguities in the phase data, resulting in an unwrapped phase band. This phase unwrapping process removes the discontinuities present in the wrapped phase, allowing for more accurate representation of surface deformations. After the import of the product, the interferometric phase was converted into displacement phase using the phase to displacement option as per the results shown in fig. 6.

Due to the natural variations in terrain elevation and the inclined viewing angle of the satellite sensor, synthetic aperture radar (SAR) images often exhibit distortions in the spatial dimensions. These distortions affect the accuracy of distance measurements within the image, resulting in a geometric representation that may not accurately reflect the real-world landscape. Terrain correction processes are designed to mitigate these effects, ensuring that the final image aligns as closely as possible with the true Earth's surface. For geocoding Sentinel-1 products, we will employ the Range Doppler Terrain Correction operator, which applies the Range Doppler orthorectification method. This advanced technique corrects geometric distortions by accounting for both the satellite's motion and the terrain's elevation, producing a more precise geospatial representation of the imaged area. The terrain corrected Dem is shown in fig. 7.

Using SNAP for earthquake analysis yields several critical outputs that provide valuable insights into seismic events. The primary results include interferograms, which display phase differences between SAR images taken before and after the earthquake, revealing ground displacement patterns. After phase unwrapping, these interferograms produce continuous displacement maps, showing the exact magnitude of ground movement. The initial interferogram represents the phase difference between two SAR images taken before and after the earthquake. This phase difference is wrapped, meaning it contains discontinuities (phase cycles) that correlate to changes in ground displacement. The interferogram visually depicts areas of relative ground motion, highlighting potential zones of subsidence or uplift caused by the earthquake. It typically appears as a colorful pattern of fringes, where each fringe corresponds to a specific amount of ground displacement (usually multiples of 2.8 cm for Sentinel-1) (Fig. 8).

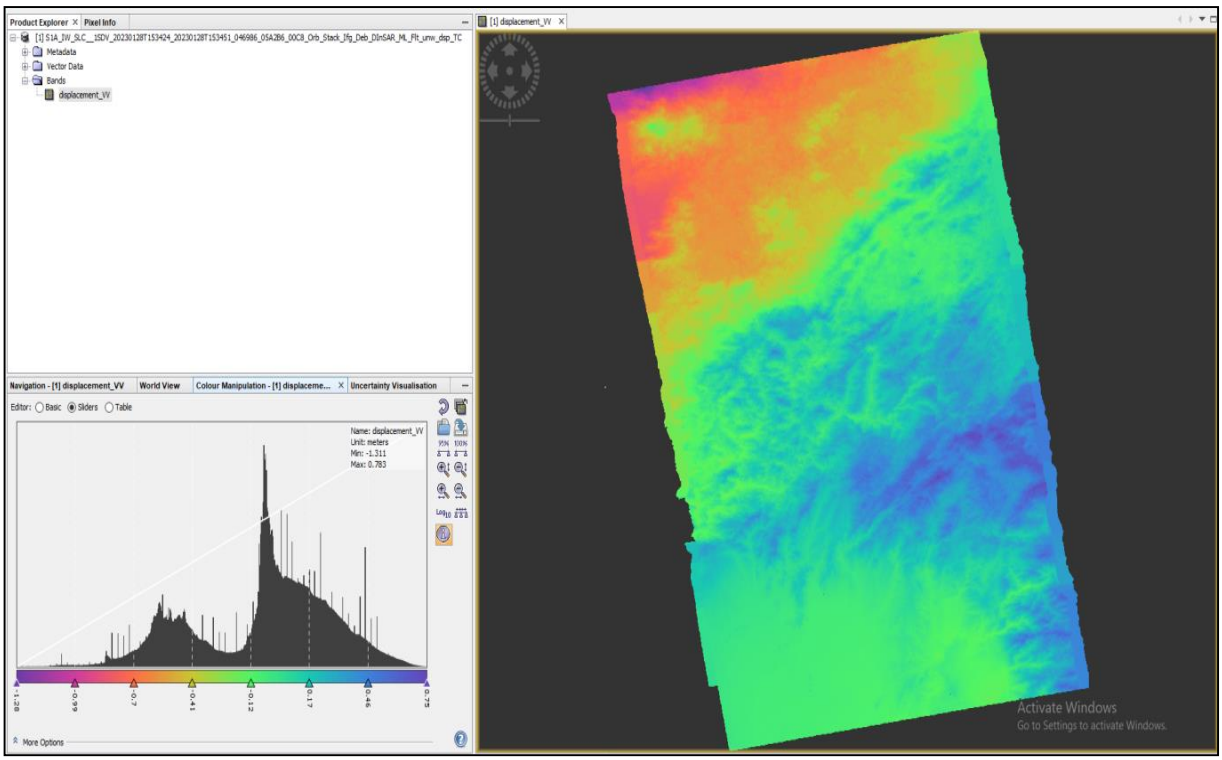

Fig. 7: Terrain corrected DEM of the Study area.

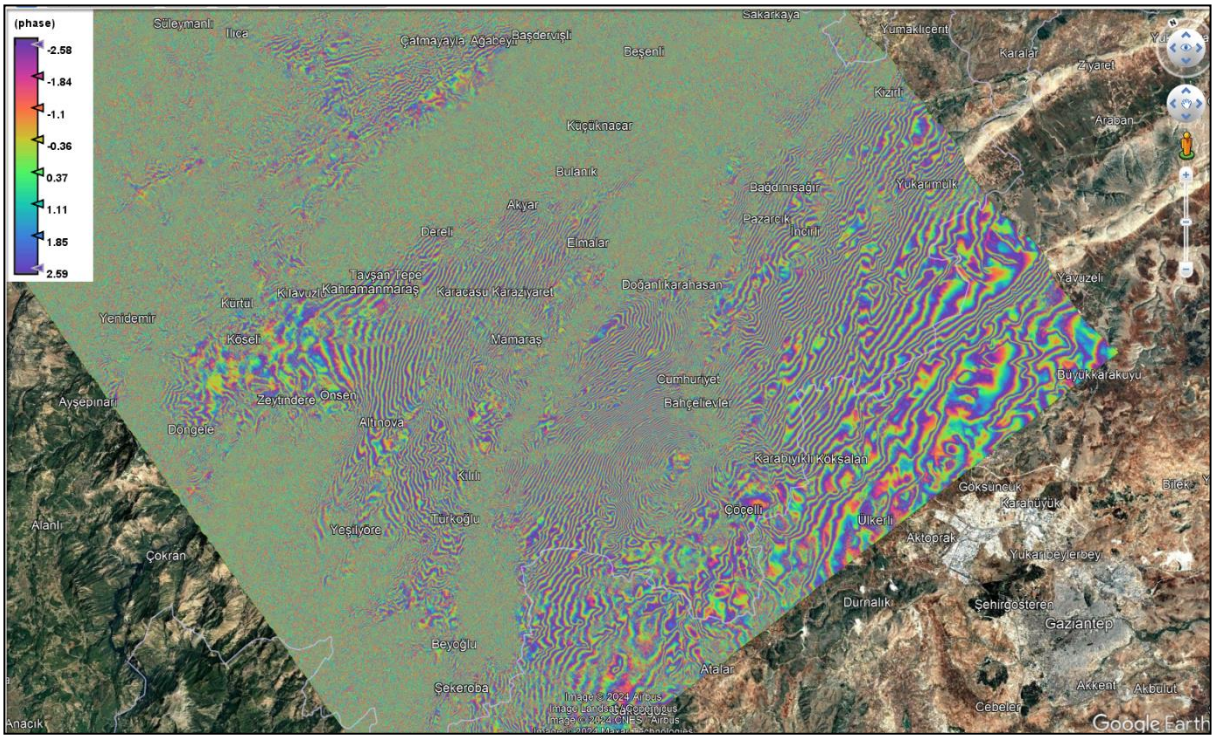

Fig. 8: The phase final output exported as KMZ file.

Conclusion

The use of ESA's Sentinel Application Platform (SNAP) for processing Synthetic Aperture Radar (SAR) data has proven to be a powerful approach in analyzing and understanding the impact of earthquakes. By leveraging the advanced tools within SNAP, such as the interferometric synthetic aperture radar (InSAR) workflow, it is possible to detect and quantify surface deformations caused by seismic events with high accuracy.

(i) Surface Deformation Detection: SNAP enables the creation of interferograms from Sentinel-1 SAR images, which reveal ground displacement patterns in earthquake-affected regions. Through phase analysis and phase unwrapping using tools like SNAPHU, significant surface displacements (both vertical and horizontal) can be measured with sub-centimeter accuracy. This helps in identifying fault lines and understanding the scale of tectonic activity.

(ii) Accurate Terrain Correction: One of the challenges in processing SAR data over earthquake regions is correcting for distortions caused by terrain variations. The Range Doppler Terrain Correction tool available in SNAP efficiently compensates for topographic distortions by integrating digital elevation models (DEMs). This ensures that the georeferenced output matches the actual geographical location, enhancing the precision of surface displacement measurements.

(iii) Interferometric Analysis for Subsidence and Uplift: SNAP-based processing allows for detailed interferometric analysis, which is crucial for monitoring land subsidence and uplift due to seismic shifts. The differential interferometric SAR (DInSAR) technique enables the identification of subtle changes in the Earth's surface over time, making it possible to assess long-term deformation trends post-earthquake.

(iv) Comprehensive Data Integration: SNAP's ability to integrate different data sources, including Sentinel-1 SAR and auxiliary datasets (e.g. DEMs, optical data), enhances the depth of analysis. The combination of SAR and optical data provides a more complete picture of earthquake impacts, aiding in both short-term response efforts and long-term seismic hazard assessment.

(v) Accessibility and Automation: The open-source nature of SNAP and its modular processing chains allow for reproducible, automated workflows, making it an accessible tool for earthquake research. The platform's flexibility allows researchers and disaster management agencies to conduct rapid assessments of earthquake damage across large areas in near-real-time.

(vi) Improvement in Earthquake Early Warning Systems: Through the detailed analysis of ground displacement and fault line movement, SNAP-based SAR processing contributes to improving earthquake early warning systems and risk mitigation strategies. The detection of pre- and post-seismic ground deformation patterns enhances the understanding of fault dynamics, potentially offering insights into future seismic activity.

In conclusion, the application of SNAP for earthquake studies is invaluable for mapping ground displacement, understanding fault behavior and supporting disaster response efforts. The platform's comprehensive set of tools, combined with Sentinel-1's regular data acquisitions, allows for the generation of highly accurate deformation maps that can inform both scientific research and practical applications in seismic hazard management.

References

1. Akhmadiya Asset, Moldamurat Khuralay, Nabi Nabiyev and Aigerim Kismanova, Application of GMTSAR and ESA SNAP Software to Determine Earthquake Epicenter Coordinate Using Sentinel-1A/B Radar Remote Sensing Data, Doi: 10.1109/SIST50301.2021.9465906 **(2021)**

2. Ardzilla Zulfha, Kurniadin Nia, Astrolabe Prasetya F.V., Wumu Romansah, Arifin Dawamul and Suryalfihra Shabri, Detection of the Post-Earthquake Damage in Mamuju Regency in January 2021 Using Sentinel-1 Satellite Imagery, *Buletin Poltanesa*, **24(1)**, 100-108, Doi: 10.51967/tanesa.v24i1.2495 **(2023)**

3. Babji Prasad Ch., Geethamma T. and Prabhakar T., Wireless Technologies on the road to effective Disaster Management: A survey, *Disaster Advances*, **17(1)**, 62-72 **(2024)**

4. Barnum H.N., Earthquake in eastern Turkey, *The Independent* **(1893)**

5. Bayar Güzin, Economic Effects of Earthquakes: 1999 Marmara/Türkiye Earthquake Case, *Ege Academic Review*, **25**, 455-474, Doi: 10.21121/eab.20250213 **(2025)**

6. Bozkurt E., Neotectonics of Turkey – a synthesis, *Geodinamica Acta*, **14**, 3–30 **(2001)**

7. Brimzhanova S., Akhmadiya A., Nabiyev N. and Moldamurat Khuralay, Determination of the earthquake epicenter using the maximum displacement method obtained by Sentinel-1A/B data via ESA SNAP software, *Bulletin of the National Engineering Academy of the Republic of Kazakhstan*, **84**, 55-69, Doi: 10.47533/2020.1606-146X.154 **(2022)**

8. Çaksen Hüseyin, A Spiritual Lesson to be Taken from the Earthquake in Türkiye, *Pakistan Journal of Medical and Health Sciences*, **18**, Doi: 10.53350/pjmhs020241811.1 **(2025)**

9. Cemali Mustafa, Arslan Başak, Öztürk Demet, Sarı Mustafa, Alataş Duygu, Cimilli Elif and Karaduman Aynur, Examining the earthquake-related experiences of people who experienced the earthquake in Turkey, *International Journal of Social Psychiatry*, Doi: 10.1177/002076402413060 **(2024)**

10. Elmas A. and Yiğitbaş E., Ophiolite emplacement by strike-slip tectonics between the Pontide Zone and the Sakarya Zone in northwestern Anatolia, Turkey, *International Journal of Earth Sciences*, **90**, 257-269 **(2001)**

11. Erler A., Tectonic setting of the massive sulfide deposits of the Southeast Anatolian Thrust Belt, In Tekeli O. and Göncüoğlu M.C., eds., International Symposium on the Geology of the Taurus Belt, MTA Publ., 237–244 **(1984)**

12. Floyd P.A., Göncüoğlu M.C., Winchester J.A. and Yalınız M.K., Geochemical character and tectonic environment of Neotethyan ophiolitic fragments and metabasites in the Central Anatolian Crystalline Complex, Turkey, In Bozkurt E., Winchester J. and Piper J.A., eds., Tectonics and Magmatism in Turkey and the Surrounding Area, Geol. Soc. London Spec. Publ., **173**, 183–202 **(2000)**

13. Görür N., Tüysüz O. and Şengör A.M.C., Tectonic evolution of the Central Anatolian Basins, *International Geology Review*, **40**, 831-850 **(1998)**

14. Koçyiğit A., Yılmaz A., Adamia S. and Kuloshvili S., Neotectonics of East Anatolian Plateau (Turkey) and Lesser Caucasus: implication for transition from thrusting to strike-slip faulting, *Geodinamica Acta*, **14**, 177-195 **(2001)**

15. Lomax A., Precise, NLL-SSST coherence hypocenter catalog for the 2023 Mw 7.8 and Mw 7.6 SE Turkey earthquake sequence (v3.0), Zenodo, Doi: 10.5281/zenodo.8089273 **(2023)**

16. Satoh Toshimi, Characterized source model of the 2023 Mw 7.6 Turkey earthquake for strong motion prediction of crustal mega-earthquakes, *Earth, Planets and Space*, **77**, Doi: 10.1186/s40623-025-02191-z **(2025)**

17. Tan Fengzhou, Kao Honn, Nissen Edwin and Visser Ryan, Tracking earthquake sequences in real time: Application of Seismicity-Scanning based on Navigated Automatic Phase-picking (S-SNAP) to the 2019 Ridgecrest, California sequence, *Geophysical Journal International*, **223**, 1511-1524, Doi: 10.1093/gji/ggaa387 **(2020)**.

(Received 29th May 2025, accepted 27th July 2025)